

## Chapter 2

# Atom–Light Interactions for Independent Atoms

The purpose of this chapter is to introduce from a fundamental level the model for atom-light interactions that is used in much of the rest of this work. We will introduce a fully quantitative model of the atom-light interaction in thermal alkali-metal vapour that can be used to make predictions for and be compared to experimental spectroscopic data.

We will start our discussion with the most basic of systems, that of an oscillator with two levels coupled by a near-resonant driving field, before adding in the full atomic structure and motional effects.

The development of this model in the atomic and molecular physics group at Durham over recent years has led to a plethora of research [1–7], and this chapter summarises some of that work. In the next chapter we will expand this model to cover the additional complexities of spectroscopy in nano-cells, and in Chap. 5 we will add the effects of the dipole–dipole interaction. It is therefore important that the underlying model is well understood.

### 2.1 The Two-Level Atom

We start our discussion of atom-light systems by looking at the case where the atom has only two levels, coupled by a near-resonant monochromatic light source. Figure 2.1 shows a typical level scheme for the two level system.

We assume for simplicity in this picture that there is no decay out of the ground state. The ground and excited states are coupled by a near-resonant laser with Rabi frequency  $\Omega$ . The excited state spontaneously decays, at a characteristic rate  $\Gamma_0$ , and the atom can only return to the ground state. For the first excited states of Rb,  $\Gamma_0 \approx 2\pi \times 6$  MHz. The detuning  $\Delta$  is the difference in angular frequencies between the laser ( $\omega_p$ ) and atomic resonance ( $\omega_0$ ) frequencies,  $\Delta = \omega_p - \omega_0$ .

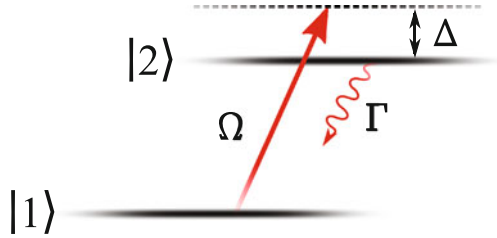


**Fig. 2.1** Schematic of the 2-level atom. Ground- ( $|1\rangle$ ) and excited-states ( $|2\rangle$ ) are coupled by a near-resonant laser with angular frequency  $\omega_p$ , driving Rabi frequency  $\Omega$ , and detuned by  $\Delta = \omega_p - \omega_0$  from resonance. The excited state spontaneously decays at a rate  $\Gamma_0$

A full many-body quantum mechanical treatment of this system is intractable due to the large numbers involved<sup>1</sup> so we must employ some approximations. The first is known as the semiclassical approximation, where a quantised atomic system is coupled to a classical electromagnetic field, valid for large photon numbers. The atom-light interaction is then between the applied field and the electric dipole moment of the atom and we neglect higher order multipole terms—this is known as the electric-dipole approximation.

Since the atom number is intractably large, we need a statistical method of describing the properties of the system. The density matrix formalism provides such a description. As the orthonormal basis states  $\{|i\rangle\}$  form a complete set, we can describe an individual quantum state of the system as a superposition of basis states

$$|\psi^s\rangle = \sum_i C_i^s |i\rangle, \quad (2.1)$$

where the  $C_i^s$  coefficients are probability amplitudes of being in the basis state  $|i\rangle$ . When the system is in a mixed state it is not possible to describe it in terms of a ket vector. In this case we can use the density matrix, defined as

$$\rho = \sum_s p(s) |\psi^s\rangle \langle \psi^s|, \quad (2.2)$$

where  $p(s)$  is the probability of the pure state  $s$ . For an  $n$ -level system, the density matrix is an  $n$ -by- $n$  matrix where the diagonal terms  $\rho_{nn}$  represent the populations of each level and the off-diagonal terms  $\rho_{mn}$  correspond to the coherences between levels.

One can calculate the expectation value of the Hamiltonian (or any other operator) from

<sup>1</sup> For typical experimental parameters, we have  $10^{22}$  atoms/m<sup>3</sup>, a focal spot size  $\sim 10$   $\mu$ m and a cell thickness of  $0.5$   $\mu$ m, which gives roughly  $10^6$  atoms.  $1$  nW of incident laser power corresponds to roughly  $10^9$  photons per second and an intensity of  $1$  mW/cm<sup>2</sup>.

$$\langle \hat{\mathcal{H}} \rangle = \text{Tr}(\rho \hat{\mathcal{H}}), \quad (2.3)$$

where the trace is defined in the usual way as  $\text{Tr}(\hat{A}) = \sum_i A_{ii}$ .

### 2.1.1 Hamiltonian

We want to calculate the time evolution of the atom-light system, so the problem we need to solve is a Schrödinger-type equation where the Hamiltonian of the combined atom-light system is given by the sum of the atomic Hamiltonian  $\hat{\mathcal{H}}^a$  and the Hamiltonian due to the interaction with the light field  $\hat{\mathcal{H}}^i$

$$\hat{\mathcal{H}} = \hat{\mathcal{H}}^a + \hat{\mathcal{H}}^i. \quad (2.4)$$

We can describe the system in terms of the orthogonal basis states that make up the bare (unperturbed) atomic states (i.e. solutions to the time-independent Schrödinger equation  $\hat{\mathcal{H}}^a|i\rangle = E_i|i\rangle$ ). The Hamiltonian can be expressed in matrix form, with elements

$$\mathcal{H}_{ij} = \langle i|\hat{\mathcal{H}}|j\rangle. \quad (2.5)$$

The atomic part of the Hamiltonian contains information about the energies of the states. Setting the ground state energy as the zero of the energy scale, we have

$$\hat{\mathcal{H}}^a = \begin{pmatrix} 0 & 0 \\ 0 & \hbar\omega_0 \end{pmatrix}. \quad (2.6)$$

The interaction Hamiltonian in the dipole approximation is given as

$$\hat{\mathcal{H}}^i = -\hat{\boldsymbol{\mu}} \cdot \boldsymbol{\mathcal{E}}, \quad (2.7)$$

where  $\hat{\boldsymbol{\mu}} = e \hat{\mathbf{r}}$  is the dipole operator, which has only off-diagonal elements (the diagonal terms  $\langle 1|\hat{\boldsymbol{\mu}}|1\rangle = \langle 2|\hat{\boldsymbol{\mu}}|2\rangle = 0$  due to the parity of the states<sup>2</sup>). For monochromatic light the electromagnetic field,  $\boldsymbol{\mathcal{E}}$ , can be expressed as

$$\boldsymbol{\mathcal{E}} = \hat{\mathbf{e}}\mathcal{E}_0 \cos(\omega_p t) = \frac{\hat{\mathbf{e}}\mathcal{E}_0}{2} (e^{i\omega_p t} + e^{-i\omega_p t}), \quad (2.8)$$

where  $\hat{\mathbf{e}}$  is a vector describing the polarisation of the field. Assuming the dipole moment is aligned with the field, the components of the interaction Hamiltonian can then be expressed as

---

<sup>2</sup> In the wavefunction representation, the matrix element between an initial and final state is given by  $\langle f|\hat{\boldsymbol{\mu}}|i\rangle = e \int_{-\infty}^{+\infty} \psi_f^*(\mathbf{r}) \mathbf{r} \psi_i(\mathbf{r}) d\mathbf{r}$ . The dipole operator is an odd function, therefore for this integral to be non-zero, the two states need to be of opposite parity.

$$\mathcal{H}_{21}^i = \mathcal{H}_{12}^{i*} = -\frac{d_{21}\mathcal{E}_0}{2}(e^{-i\omega_p t} + e^{i\omega_p t}). \quad (2.9)$$

The first term in Eq. (2.9) represents the interaction when either the system absorbs a photon and is raised to the excited state, or when the system emits a photon and falls to the ground state from the excited state. The second term is known as the counter-rotating term, associated with the simultaneous absorption of a photon and falling from the excited to ground state, or when the system emits a photon and is raised to the excited state. These second terms are omitted from the rest of the analysis, an approximation known as the Rotating Wave Approximation (RWA) [8]. When the problem is transformed into a rotating frame, we see that the omitted terms are those owing to the ‘fast’ oscillations, which evolve as  $e^{i(\omega_0+\omega_p)t}$ , and average away to zero. We are left with the ‘slow’ oscillations, which evolve as  $e^{i(\omega_0-\omega_p)t} = e^{-i\Delta t}$ , which do not average away.

The total Hamiltonian can therefore be rewritten in the RWA as

$$\hat{\mathcal{H}} = \hbar \begin{pmatrix} 0 & \frac{\Omega}{2} e^{i\omega_p t} \\ \frac{\Omega}{2} e^{-i\omega_p t} & \omega_0 \end{pmatrix}. \quad (2.10)$$

where the Rabi frequency  $\Omega$  is given by

$$\Omega = -\frac{\boldsymbol{\mu}_{21} \cdot \hat{\mathbf{e}}\mathcal{E}_0}{\hbar} = -\frac{e\mathcal{E}_0}{\hbar} \langle 1|\mathbf{r}|2\rangle, \quad (2.11)$$

and we have assumed that the polarisation of the driving field is aligned with the atomic dipole moment.

### 2.1.2 Time Evolution

The time evolution of the system can then be calculated from the time dependent Schrödinger equation, which for the density matrix is equivalent to solving

$$\frac{d}{dt}\rho = \frac{1}{i\hbar} [\hat{H}, \rho], \quad (2.12)$$

the Liouville-von Neumann equation. However, this does not account for decay in the system due to, for example, spontaneous emission. Decay is added in phenomenologically as a statistical process, grouped into the decay matrix  $\mathcal{L}$ . The equation that must be solved is known as the Linblad master equation, and is given by

$$\frac{d}{dt}\rho = \frac{1}{i\hbar} [\hat{H}, \rho] - \mathcal{L}. \quad (2.13)$$

For the two level system, the steady state solutions can be derived analytically, which we do by writing (2.13) as a set of coupled rate equations known as the Optical Bloch Equations (OBE). For the two level system with dephasing due only to spontaneous decay, these are

$$\begin{aligned} \frac{d\rho_{11}}{dt} &= -\frac{d\rho_{22}}{dt} \\ &= \Gamma_0\rho_{22} - \frac{i\Omega}{2}(\tilde{\rho}_{21} - \tilde{\rho}_{12}) \end{aligned} \quad (2.14)$$

$$\begin{aligned} \frac{d\tilde{\rho}_{21}}{dt} &= \frac{d\tilde{\rho}_{12}^*}{dt} \\ &= -(\Gamma_0/2 - i\Delta)\tilde{\rho}_{21} - \frac{i\Omega}{2}(\rho_{11} - \rho_{22}), \end{aligned} \quad (2.15)$$

where we have introduced the ‘slow’ variables in the coherence terms,  $\tilde{\rho}_{21} = \tilde{\rho}_{12}^* = \rho_{21}e^{-i\omega_p t}$ . To conserve population, we must have  $\rho_{11} + \rho_{22} = 1$ , and clearly  $d\rho_{11}/dt + d\rho_{22}/dt = 0$ . In the steady state,  $d\rho/dt = 0$ , and we thus find

$$\tilde{\rho}_{21} = -\frac{i\Omega/2}{\Gamma_0/2 - i\Delta}(\rho_{11} - \rho_{22}). \quad (2.16)$$

## 2.2 Electric Susceptibility

We can describe the optical response of the atomic system to an applied light field in terms of the complex electric susceptibility,  $\chi$ , which describes how the medium polarises in response to an applied electric field. The macroscopic polarisation of the medium is related to the individual electric dipole moments of the atoms. For an ensemble we take the average dipole moment and obtain

$$\mathbf{P} = N\langle\hat{\boldsymbol{\mu}}\rangle = N\boldsymbol{\mu}_{21}[\rho_{21}e^{-i\omega_p t} + \rho_{12}e^{i\omega_p t}], \quad (2.17)$$

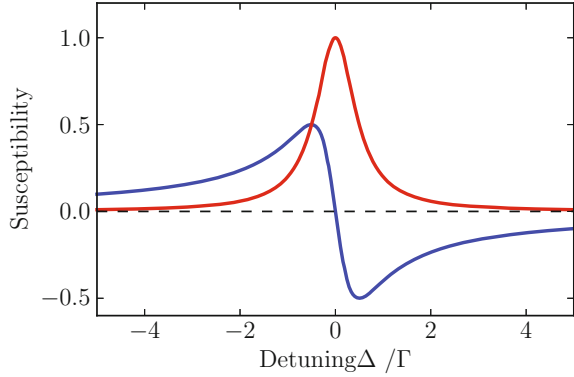
where  $N$  is the atomic density. The polarisation is related to the complex linear susceptibility by [9]

$$\mathbf{P} = (\epsilon - \epsilon_0)\mathcal{E} = \epsilon_0\chi\mathcal{E} \quad (2.18)$$

$$= \frac{\epsilon_0\mathcal{E}_0}{2}[\chi e^{-i\omega_p t} + \chi^* e^{i\omega_p t}], \quad (2.19)$$

assuming  $\mathcal{E}_0$  is real. We combine Eqs. (2.17) and (2.19) and take the dot product with  $\boldsymbol{\mu}_{21}$ , yielding

**Fig. 2.2** Real (blue) and imaginary (red) parts of the linear susceptibility for a two-level atom around a resonance



$$N\mu_{21}^2(\tilde{\rho}_{21}e^{-i\omega_p t} + \tilde{\rho}_{12}e^{i\omega_p t}) = -\frac{1}{2}\epsilon_0\hbar\Omega(\chi e^{-i\omega_p t} + \chi^* e^{i\omega_p t}). \quad (2.20)$$

We then find a relationship between the susceptibility and the coherence term in the density matrix

$$\chi = -\frac{2N\mu_{21}^2}{\epsilon_0\hbar\Omega}\tilde{\rho}_{21}. \quad (2.21)$$

Combining this with Eq. (2.16), in the weak probe limit, where  $\Omega \ll \Gamma_0$  and we assume all the population remains in the ground state ( $\rho_{11} - \rho_{22} \approx 1$ ), we obtain as a function of the laser detuning

$$\chi(\Delta) \simeq \frac{iN\mu_{21}^2}{\epsilon_0\hbar(\Gamma_0/2 - i\Delta)}. \quad (2.22)$$

In the absence of any other broadening mechanism, this has real and imaginary components with the classic dispersive and Lorentzian lineshapes, as shown in Fig. 2.2. The refractive index of the medium is related to its relative dielectric constant  $\epsilon_r$  and thus the susceptibility of the medium,  $n = \sqrt{\epsilon_r} = \sqrt{1 + \chi}$ .

It should be noted that since much of this work deals with large susceptibilities, the usual approximation of  $n \approx 1 + \chi/2$  does not hold. Once the susceptibility becomes large, local field effects need to be considered (discussed in Chap. 5). If one does not consider local field effects,  $\sqrt{1 + \chi(\Delta)}$  is no longer symmetric about  $\Delta = 0$  and one might mistakenly identify a fictitious blue-shift of the lines (see Appendix D).

A monochromatic electric field propagating through a medium with a (isotropic) refractive index  $n$  and thickness  $\ell$  will be attenuated and phase-shifted so that at the output the field will be given by

$$\mathcal{E}_{\text{out}} = \mathcal{E}_{\text{in}}e^{inkz} = \mathcal{E}_{\text{in}}e^{-n_I kz}e^{i n_R kz}, \quad (2.23)$$

where  $n_{R,I}$  are the real and imaginary parts of the refractive index,  $k = 2\pi/\lambda$  is the wavenumber with  $\lambda$  the transition wavelength. The output intensity (the measurable quantity) is then

$$I_{\text{out}} = |\mathcal{E}_{\text{out}}|^2 = I_{\text{in}} e^{-2n_I k z}, \quad (2.24)$$

which is just the Beer-Lambert law with the absorption coefficient  $\alpha = 2n_I k$ . The frequency dependent transmission is then  $\mathcal{T} = I_{\text{out}}/I_{\text{in}}$ .

### 2.3 Motion and the Doppler Effect

So far we have only dealt with stationary atoms. In any room temperature ensemble, the atoms have thermal velocity  $v$ , typically around 250 m/s for room temperature atoms. The frequency of light absorbed by the atom is therefore Doppler shifted according to the velocity of the atom, by an amount

$$\Delta_D = -\mathbf{k} \cdot \mathbf{v} = -k v_z, \quad (2.25)$$

where  $\mathbf{k}$  is the wavevector of the incoming (monochromatic) laser beam, taken to be along the  $z$ -axis. We see immediately from this relation that it is only when there is a component of velocity in the axis of the beam  $v_z$  that there is any shift in frequency. Since atomic velocities are distributed in all directions, there are a range of velocities which interact resonantly with the laser beam. In one dimension (along the axis of the beam), a Maxwellian distribution of velocities is assumed such that the atomic density for a given velocity class  $N(v)$  is given by

$$N(v) = \frac{N_0}{u\sqrt{\pi}} e^{-v^2/u^2}, \quad (2.26)$$

with the most probable velocity  $u = \sqrt{2k_B T/m}$  where  $m$  is the mass of the atoms and  $T$  their absolute temperature, and we have dropped the  $z$  subscripts since we are only dealing with one dimension.

Atoms moving away from a blue-detuned laser beam are Doppler shifted back onto resonance and thus absorb the light, and similarly for a red-detuned laser and atoms moving into the beam. The resonance condition is fulfilled wherever  $\Delta + kv = 0$ . This leads to an inhomogeneous broadening of the absorption line, with a characteristic Doppler width  $\delta\omega_d$ , which for hot atoms is significantly larger than the natural linewidth. This places a limit on the spectral resolution, such that features separated by less than the Doppler width are not resolved. For  $^{85}\text{Rb}$  atoms at room temperature, the Doppler width  $\Gamma_D \approx 2\pi \times 500$  MHz, and so the hyperfine structure lines on the D2 line separated by  $\sim 2\pi \times 100$  MHz cannot ordinarily be resolved. To obtain sub-Doppler resolution, usual spectroscopic methods involve a second pump beam (such as saturated absorption/hyperfine pumping spectroscopy [10] or

polarisation spectroscopy [11, 12]), although sub-Doppler resolution is possible in a nano-cell without a second beam—this will be expanded upon in Chap. 3.

Adding in Doppler broadening to the formulae in Sect. 2.2 is a relatively simple process. We make the following modifications to Eq. (2.22):

$$\begin{aligned}\Delta &\rightarrow \Delta - kv \\ N &\rightarrow N_{\text{vc}}(v)\end{aligned}$$

We then must take into account all velocities, so we have, as a function of the laser detuning

$$\chi(\Delta, v) \simeq \frac{iN_{\text{vc}}(v)\mu_{21}^2}{\epsilon_0\hbar(\Gamma_0/2 - i(\Delta - kv))} \quad (2.27)$$

$$\chi(\Delta) \simeq \int \chi(\Delta, v)dv. \quad (2.28)$$

The lineshape that this convolution produces is known as the Voigt profile, and is discussed in the next section.

## 2.4 Lineshapes: Lorentzians, Gaussians and the Voigt Profile

The lineshape associated with the light absorption of an ensemble of thermal atoms is a Voigt profile. Mathematically, this is the convolution of a Gaussian, from the Doppler broadening, with a Lorentzian, from the homogeneous natural linewidth,  $\Gamma_0$ . Additional sources of broadening (such as dipole–dipole interactions, which will be discussed later) can also be included by further convolving with the appropriate lineshape. For sources of homogeneous (i.e. all atoms see the same effect) broadening, their lineshape is another Lorentzian. In this case we can take advantage of the fact that a convolution of two Lorentzians with widths  $w_1$  and  $w_2$  is another Lorentzian with width  $w_1 + w_2$ , which makes computation significantly faster since convolution routines are slow and scale badly with the length of the arrays used.

It is important to understand the relative importance of the various broadening mechanisms. In terms of the vapour temperature there are a few regimes of interest, shown in panels (a–c) of Fig. 2.3. For experiments with cold and ultra-cold atoms (panel (a), calculated here for  $T = 1$  mK), we expect the atomic motion to have little effect and therefore the Voigt profile is well approximated as a Lorentzian with natural linewidth  $\Gamma_0$ . As temperature increases there is then a regime where neither Lorentzian nor Gaussian approximations fit well. As temperature increases to room-temperature (b), the Doppler effect is significant and near resonance the lineshape can be well approximated by a Gaussian with width  $\Gamma_D$ . Out in the wings of the resonance however, the Lorentzian component still has a measurable effect [13] owing to the relative scaling of the two functions with detuning. This becomes increasingly

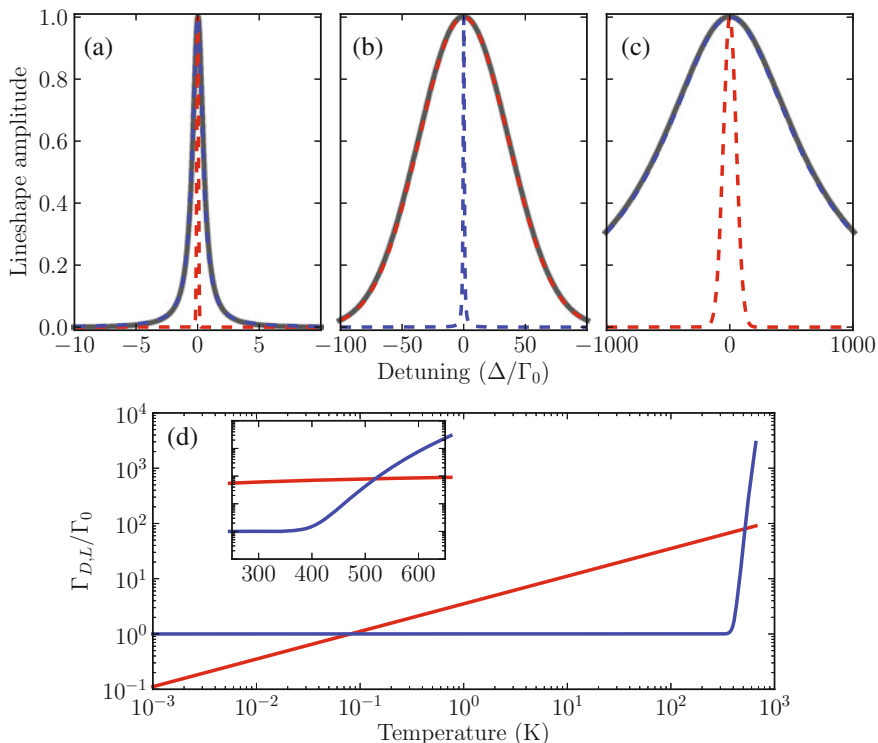


**Fig. 2.3** (a–c) A comparison between the Voigt profile (*black*) and the Lorentzian (*dashed blue*) and Gaussian (*dashed red*) components. For cold atoms (a), the motion of the atoms can be neglected and the Voigt is well approximated by a Lorentzian whose width is the natural atomic linewidth  $\Gamma_0$ . At room temperature (b) Doppler broadening dominates and the Voigt is well approximated by a Gaussian, while for temperatures in excess of  $\sim 300$  °C (c) the Lorentzian component due to dipole-dipole interactions dominates (the inset shows an expanded view of the crossing). Panel (d) shows the relative widths of the Lorentzian ( $\Gamma_L = \Gamma_0 + \Gamma_{dd}$ ) and Gaussian ( $\Gamma_D$ ) components as a function of temperature, where the near-exponential dependence on temperature of atom-atom interactions can be seen clearly

important as temperature rises further. The contribution to the Lorentzian width from dipole-dipole interactions,  $\Gamma_{dd}$ , sharply increases owing to the linear dependence on number density and hence near-exponential dependence on temperature (see Chap. 5). In this regime ( $T \approx 150$ – $300$  °C) we again have a regime where the full Voigt lineshape is approximated badly by both Gaussian and Lorentzian profiles.

The final regime, shown in panel (c), involves very hot ( $T \gtrsim 300$  °C) and therefore very dense atomic gases. In this regime, the interactions between atoms dominate over all other line broadening mechanisms and the lineshape can once again be well approximated by only a Lorentzian function with width  $\Gamma_L \approx \Gamma_{dd}$ . Panel (d) compares the widths of the Lorentzian,  $\Gamma_L = \Gamma_0 + \Gamma_{dd}$ , and Gaussian  $\Gamma_D$  components as a function of temperature.

## 2.5 Atomic Structure

It should be clear that for any real system, the above discussion is an idealised model. For the alkali metal atoms, the single valence electron means that the atomic structure is still relatively simple. For the ground state transitions, commonly known as the D1 ( $5S_{1/2} \rightarrow 5P_{1/2}$ ) and D2 ( $5S_{1/2} \rightarrow 5P_{3/2}$ ) lines, there are many allowed transitions between the hyperfine energy levels. The probability amplitude for each transition is found from the dipole matrix element of that transition. In the  $F$  basis, with Zeeman sub-levels  $m_F$ , the matrix element is  $\langle F_g, m_{F_g} | e r | F_e, m_{F_e} \rangle$  for a transition between a ground state  $g$  and excited state  $e$ . In this thesis, we do not deal with applied magnetic fields and neglect the Earth’s magnetic field, so we can just consider the transition between  $F$ -states. The transition probabilities  $|\langle F_g | e r | F_e \rangle|^2$  are then the Clebsch–Gordan coefficients, which can be found tabulated for the Rb D1 and D2 lines in [1]. In addition, Rb has two common stable isotopes,  $^{85}\text{Rb}$  with a natural abundance of  $\approx 72\%$  and  $^{87}\text{Rb}$  with a natural abundance of  $\approx 28\%$ , so this adds a factor of two to the number of transitions.

It is possible to model the full dynamics of this system by solving an  $\mathcal{N}$ -level version of the master equation (Eq. (2.13)), but this is computationally intensive as there are  $\mathcal{N}^2$  coupled equations to solve. The model we use considers only the effect of a weak probe on the system, so optical pumping between levels is negligible. It is therefore assumed that every transition is effectively its own separate two-level system separated in frequency space by the atomic hyperfine structure, and we simply sum over all the dipole-allowed transitions, weighted by their transition probabilities, to calculate the susceptibility at a given laser detuning. This approach has been successful in predicting the full spectrum of the Rb D1 and D2 lines in the past, with agreement between experiment and theory at the 1% level [1]. Using a more involved model to find the transition amplitudes in the  $|m_L, m_S, m_I\rangle$  uncoupled basis has also yielded fruitful results when considering the effect of magnetic fields up to 0.6 T [14–16], with excellent agreement between experiment and theory.

## 2.6 Summary

The development of a simple model that accurately reproduces experimental spectra has been key to a great deal of research in the Durham atomic and molecular physics group. It is not only a useful tool, in terms of fitting data and extracting parameters, but also gives an ability to predict novel effects. Implementing this principle for very high magnetic fields has led to the development of an atom-based optical isolator [16]; a dichroic beamsplitter based on the Faraday effect [4]; and a tool for off-resonance laser locking at arbitrary frequencies [5].

One of the goals for this work was to extend this model to the subtleties and extra complications introduced by the confinement of atoms in nano-cells, which will be the subject of the next chapter.

## References

1. P. Siddons, C.S. Adams, C. Ge, I.G. Hughes, Absolute absorption on rubidium d lines: comparison between theory and experiment. *J. Phys. B* **41**, 155004 (2008)
2. P. Siddons, N.C. Bell, Y. Cai, C.S. Adams, I.G. Hughes, A gigahertz-bandwidth atomic probe based on the slow-light faraday effect. *Nat. Photon* **3**, 225 (2009)
3. P. Siddons, C.S. Adams, I.G. Hughes, Optical control of faraday rotation in hot rb vapor. *Phys. Rev. A* **81**, 043838 (2010)
4. R.P. Abel, U. Krohn, P. Siddons, I.G. Hughes, C.S. Adams, Faraday dichroic beam splitter for raman light using an isotopically pure alkali-metal-vapor cell. *Opt. Lett.* **34**, 3071 (2009)
5. A.L. Marchant et al., Off-resonance laser frequency stabilization using the faraday effect. *Opt. Lett.* **36**, 64 (2011)
6. L. Weller, R.J. Bettles, P. Siddons, C.S. Adams, I.G. Hughes, Absolute absorption on the rubidium d1 line including resonant dipole-dipole interactions. *J. Phys. B* **44**, 195006 (2011)
7. S.L. Kemp, I.G. Hughes, S.L. Cornish, An analytical model of off-resonant faraday rotation in hot alkali metal vapours. *J. Phys. B* **44**, 235004 (2011)
8. C. Tannoudji, J. Dupont-Roc, G. Grynberg, *Atom-Photon Interactions* (Wiley, New York, 1998)
9. J. Gea-Banacloche, Y.-Q. Li, S.-Z. Jin, M. Xiao, Electromagnetically induced transparency in ladder-type inhomogeneously broadened media: theory and experiment. *Phys. Rev. A* **51**, 576 (1995)
10. D.A. Smith, I.G. Hughes, The role of hyperfine pumping in multilevel systems exhibiting saturated absorption. *Am. J. Phys.* **72**, 631 (2004)
11. C. Wieman, T. Hänsch, Doppler-free laser polarization spectroscopy. *Phys. Rev. Lett.* **36**, 1170 (1976)
12. M. Harris et al., Polarization spectroscopy in rubidium and cesium. *Phys. Rev. A* **73**, 62509 (2006)
13. P. Siddons, C.S. Adams, I.G. Hughes, Off-resonance absorption and dispersion in vapours of hot alkali-metal atoms. *J. Phys. B* **42**, 175004 (2009)
14. L. Weller, T. Dalton, P. Siddons, C.S. Adams, I.G. Hughes, Measuring the stokes parameters for light transmitted by a high-density rubidium vapour in large magnetic fields. *J. Phys. B* **45**, 055001 (2012)
15. L. Weller et al., Absolute absorption and dispersion of a rubidium vapour in the hyperfine paschenback regime. *J. Phys. B* **45**, 215005 (2012)
16. L. Weller et al., Optical isolator using an atomic vapor in the hyperfine paschen-back regime. *Opt. Lett.* **37**, 3405 (2012)



<http://www.springer.com/978-3-319-07099-5>

Collective Atom-Light Interactions in Dense Atomic  
Vapours

Keaveney, J.

2014, XIII, 144 p. 77 illus., 36 illus. in color., Hardcover

ISBN: 978-3-319-07099-5